

Ultrafast photoionization of ions and molecules by orthogonally polarized intense laser pulses: Effects of the time delay

Si-Qi Zhang(张思琪), Zhi-Jie Yang(杨志杰), Zhi-Xian Lei(雷志仙), Wei Feng(冯伟), Sheng-Peng Zhou(周胜鹏), Kai-Jun Yuan(元凯军), Xue-Shen Liu(刘学深), and Jing Guo(郭静)

Citation:CChin. Phys. B, 2021, 30 (**1**): 013201. DOI: 10.1088/1674-1056/abb30c
Journal homepage: http://cpb.iphy.ac.cn; http://iopscience.iop.org/cpb

What follows is a list of articles you may be interested in

Probing time delay of strong-field resonant above-threshold ionization

Shengliang Xu(徐胜亮), Qingbin Zhang(张庆斌), Cheng Ran(冉成), Xiang Huang(黄湘), Wei Cao(曹伟), and Peixiang Lu(陆培祥)
Chin. Phys. B, 2021, 30 (**1**): 013202. DOI: 10.1088/1674-1056/abc7a5

Resonance-enhanced two-photon ionization of hydrogen atom in intense laser field investigated by Bohmian-mechanics

Yang Song(宋阳), Shu Han(韩姝), Yu-Jun Yang(杨玉军), Fu-Ming Guo(郭福明), Su-Yu Li(李苏宇)
Chin. Phys. B, 2020, 29 (**9**): 093204. DOI: 10.1088/1674-1056/aba09e

Photoelectron imaging of resonance-enhanced multiphoton ionization and above-threshold ionization of ammonia molecules in a strong 800-nm laser pulse

Le-Le Song(宋乐乐), Ya-Nan Sun(孙亚楠), Yan-Hui Wang(王艳辉), Xiao-Chun Wang(王晓春), Lan-Hai He(赫兰海), Si-Zuo Luo(罗嗣佐), Wen-Hui Hu(胡文惠), Qiu-Nan Tong(佟秋男), Da-Jun Ding(丁大军), Fu-Chun Liu(刘福春)
Chin. Phys. B, 2019, 28 (**6**): 063201. DOI: 10.1088/1674-1056/28/6/063201

Photoelectron angular distributions of H ionization in low energy regime: Comparison between different potentials

Shu-Na Song(宋舒娜), Hao Liang(梁昊), Liang-You Peng(彭良友), Hong-Bing Jiang(蒋红兵)
Chin. Phys. B, 2016, 25 (**9**): 093201. DOI: 10.1088/1674-1056/25/9/093201

Origin of diffraction fringes in two-dimensional photoelectronmomentum distributions for single ionization of atoms in few-cycle intense laser pulses

Guo Zhi-Jian, Chen Zhang-Jin, Zhou Xiao-Xin
Chin. Phys. B, 2014, 23 (**4**): 043201. DOI: 10.1088/1674-1056/23/4/043201

Ultrafast photoionization of ions and molecules by orthogonally polarized intense laser pulses: Effects of the time delay*

Si-Qi Zhang(张思琪), Zhi-Jie Yang(杨志杰), Zhi-Xian Lei(雷志仙), Wei Feng(冯伟), Sheng-Peng Zhou(周胜鹏), Kai-Jun Yuan(元凯军), Xue-Shen Liu(刘学深)†, and Jing Guo(郭静)‡

Institute of Atomic and Molecular Physics, Jilin University, Changchun 130012, *China*

(Received 2 July 2020; revised manuscript received 13 August 2020; accepted manuscript online 27 August 2020)

We present the photoelectron momentum distributions (PMDs) and the photoelectron angular distributions (PADs) of He^+ ions, aligned H_2^+ molecules and N_2 molecules by intense orthogonally polarized laser pulses. Simulations are performed by numerically solving the corresponding two-dimensional time-dependent Schrödinger equations (TDSEs) within the single-electron approximation frame. Photoelectron momentum distributions and photoelectron angular distributions present different patterns with the time delays T_d, illustrating the dependences of the PMDs and PADs on the time delays by orthogonally polarized laser pulses. The evolution of the electron wavepackets can be employed to describe the intensity of the PADs from the TDSE simulations for N_2 molecules.

Keywords: photoelectron momentum distributions, photoelectron angular distributions, intense orthogonally polarized laser pulses, ultrafast photoionization model

PACS: 32.80.Rm, 32.80.Fb, 42.50.Hz, 42.65.Re **DOI:** 10.1088/1674-1056/abb30c

1. Introduction

The strong-field physics is a hot topic in recent years, and interaction of laser with atoms or molecules can produce different physical phenomena, including high order harmonic generation (HHG),[1–3] strong-field ionization, and nonsequential double ionization (NSDI).[4] The electron processes of molecular reaction dynamics are investigated with the rapid advances of ultrashort and ultrafast intense laser technology[5–7] in the attosecond time regime (1 as $= 10^{-18}$ s) and sub-nanometer dimensions.[8–10] The pump-probe technique is developed as a new tool in the femtosecond time regime.[11] Attosecond electron motion can be observed by monitoring photoelectron signal or photoelectron momentum distributions, for example, in the pump-probe technique, photoelectron momentum distributions are a function of the time delays between the pump pulses and the probe pulses.[12–15] In the past few years, a lot of researchers paid attention to photoelectron momentum and angular distributions of atoms and molecules which encode valuable and fruitful information about the electron dynamics.[16–18] It has been illustrated that the photoelectron momentum distributions (PMDs) of the He atom present vortex patterns,[19] which show the sensitivity of momentum distribution to the phases, time delays and the helicity of the laser pulses. Molecular photoionization of H_2^+ presents electron vortices in PMDs in the circularly polarized laser fields,[18] such vortex patterns can only be observed for counter-rotating and co-rotating circularly polarized fields. In addition, Yuan *et al.*[20,21] demonstrated the molecular photoelectron-momentum distribution (MPMD) depends on the molecular orbital symmetry.

Orthogonally polarized laser pulses are new powerful tools for steering attosecond electron motion of atoms and molecules.[22,23] The electronic dynamics of molecules in orthogonally polarized attosecond ultraviolet laser pulses has been studied before.[21,24] It has been found that molecular photoelectron momentum and angular distributions of H_2^+ molecules are sensitive to the relative phase of the laser pulses. However, the sensitivity of the ionic and molecular photoelectron momentum and angular distributions to the time delays in orthogonal polarized laser fields has not been studied. In this work, we present photoelectron momentum and angular distributions of ions and molecules by orthogonally polarized laser pulses with different time delays. The PMDs and photoelectron angular distributions (PADs) are dependent on the time delays, which are derived from the interference between coherent electron wave packets. The ultrafast photoionization model[25] and the evolution of the electron wavepackets are used to describe these results.

The paper is arranged as follows: In Section 2, we present the computational details for solving the two-dimensional (2D) time-dependent Schrödinger equation (TDSE) of He^+ ions, aligned H_2^+ molecules and N_2 molecules. In Section 3, we present and discuss the results of PMDs and PADs with different time delays. Finally, we summarize our results in Section 4. Throughout this paper, atomic units (a.u.) $e = \hbar = m_e = 1$ are used unless stated otherwise.

*Project supported by the National Natural Science Foundation of China (Grant Nos. 12074146, 21827805, 11974007, and 12074142) and the Natural Science Foundation of Jilin Province of China (Grant No. 20180101225JC).

†Corresponding author. E-mail: gjing@jlu.edu.cn

‡Corresponding author. E-mail: liuxs@jlu.edu.cn

© 2021 Chinese Physical Society and IOP Publishing Ltd

2. Numerical Methods

The corresponding 2D TDSE for the He^+ ions, aligned H_2^+ molecules, and N_2 molecules can be written as

$$i\frac{\partial\psi(\boldsymbol{r},t)}{\partial t}=\left[\frac{\boldsymbol{p}^2}{2}+V(\boldsymbol{r})+V_L(\boldsymbol{r},t)\right]\psi(\boldsymbol{r},t), \tag{1}$$

where $\boldsymbol{p}$ is the momentum of electron, and $V(\boldsymbol{r})$ is the soft-core Coulomb potential of He^+ ions, H_2^+ molecules, and N_2 molecules, which are shown in Figs. 1(a1)–(c1). The explicit expressions are given in the following.

The soft-core Coulomb potential of He^+ ions can be written as

$$V(\boldsymbol{r})=-\frac{b}{\sqrt{\boldsymbol{r}^2+a}}, \tag{2}$$

where $a=0.169$ and $b=2.0$ are the soft-core parameters, and the ionization potential of the ground state is $I_p=54.4$ eV for He^+ ions.

The soft-core Coulomb potential of H_2^+ molecules can be written as

$$V(x,y)=-\frac{1}{\sqrt{(x-\frac{R}{2})^2+y^2+c}}-\frac{1}{\sqrt{(x+\frac{R}{2})^2+y^2+c}}, \tag{3}$$

where $c=0.5$ is the soft-core parameter, R is the internuclear distance (the equilibrium internuclear distance is $R=R_e=2.0$ a.u.), and the ionization potential of the ground state is $I_p=29.9$ eV for H_2^+ molecules.

The soft-core Coulomb potential of N_2 molecules has the form[26,30]

$$V(\boldsymbol{r})=-\sum_j\frac{Z_j^{\infty}+(Z_j^0-Z_j^{\infty})\exp(-\boldsymbol{r}_j^2/\sigma_j^2)}{\sqrt{\boldsymbol{r}_j^2+a_j^2}}. \tag{4}$$

The subscript $j=1,2$ labels the nuclei at fixed positions $\boldsymbol{\rho}_j$ and $\boldsymbol{r}_j=\boldsymbol{r}-\boldsymbol{\rho}_j$, where $r=\sqrt{x^2+y^2}$. The numerator $Z_j^{\infty}+(Z_j^0-Z_j^{\infty})\exp(-\boldsymbol{r}_j^2/\sigma_j^2)$ is the position-dependent screened effective charge for the j-th nucleus, with Z_j^{∞} denoting the effective nuclear charge of the nucleus j as seen by an electron at infinite distance and Z_j^0 the bare charge of nucleus j. The value of Z_j^{∞} is derived from the Mulliken analysis performed in the *ab initio* study. Here a_j is the soft-core parameter, and σ_j characterizes the decrease of the effective charge with the molecular internuclear distance. The above parameters are same as those in Ref. [30]. The bond length R_{N-N} is set as 2.08 a.u. for N_2 molecules,[26] and the ionization potential of the ground state is $I_p=15.6$ eV for N_2 molecules.

The initial wave function of ions and molecules are obtained by the imaginary evolution method. The initial electron density distributions of the He^+ ions, H_2^+ molecules, and N_2 molecules are shown in Figs. 1(a2)–1(c2). One can see that the electron density distributions of He^+ ions is circular in the (x,y) plane, the electron density of the H_2^+ molecule is elliptical with the σ_g symmetry, and the N_2 molecule has three nodes located along the molecular R axis with the σ_g symmetry.

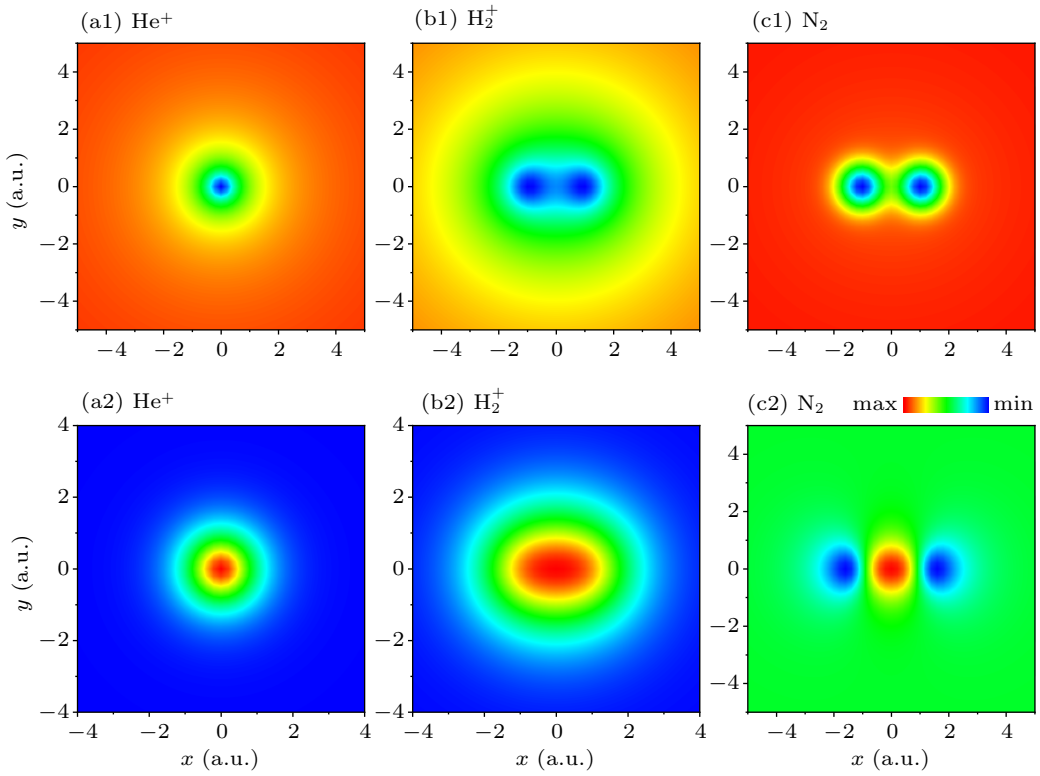


Fig. 1. Coulomb potential of (a1) the He^+ ion, (b1) the H_2^+ molecule, (c1) the N_2 molecule; and the initial ground states of (a2) the He^+ ion, (b2) the H_2^+ molecule, (c2) the N_2 molecule.

The interaction between either ions or molecules and the laser pulse is $V_L(\boldsymbol{r},t) = \boldsymbol{r}\cdot\boldsymbol{E}(t)$ with $\boldsymbol{E}(t)$ being the field vector in the (x,y) plane. The orthogonally polarized laser pulses can be expressed by

$$\begin{aligned}\boldsymbol{E}(t) &= E_x(t)\hat{e}_x + E_y(t)\hat{e}_y = E_0 f(t)\cos(\omega t)\hat{e}_x \\ &\quad + E_0 f(t-T_\mathrm{d})\cos[\omega(t-T_\mathrm{d})]\hat{e}_y, \end{aligned} \tag{5}$$

where $E_0 = 5.34\times10^{-2}$ a.u. ($I_0 = 1\times10^{14}$ W/cm^2) is the amplitude of the electric field, ω is the laser frequency, and $\hat{e}_{x/y}$ is the field polarization direction, T_d is the time delay between the two pulses, $f(t) = \sin^2(\pi t/T)$ is the pulse envelope with duration $T = 20\ T_0$, with $T_0 = 2\pi/\omega$.

The 2D TDSE is numerically solved by a second order split-operator algorithm combined with fast Fourier transform (FFT) technique[27,28]

$$\begin{aligned}\psi(\boldsymbol{r},t+\Delta t) &= \mathrm{e}^{-\mathrm{i}(\frac{\boldsymbol{p}^2}{4})\Delta t}\,\mathrm{e}^{-\mathrm{i}V(\boldsymbol{r})+\boldsymbol{r}\cdot E(t)\Delta t}\,\mathrm{e}^{-\mathrm{i}(\frac{\boldsymbol{p}^2}{4})\Delta t}\psi(\boldsymbol{r},t) \\ &\quad + O(\Delta t)^3, \end{aligned} \tag{6}$$

with time step $\Delta t = 0.01$ a.u. and the spatial steps $\Delta x = \Delta y = 0.2$ a.u. The total spatial length is 409.6 a.u., which is large enough to suppress the unphysical effects originating from the reflection of the wave packet from the boundary. During the calculation, the wave function is multiplied by a $\cos^{1/8}$ mask function in each time step, and the absorber domain ranges from $|x,y| = 150$ a.u. to $|x,y| = 204.8$ a.u. The time-dependent electronic wave function is written as $\psi(\boldsymbol{r},t)$, the ionized part is recorded as $[1-M(\boldsymbol{r})]\psi(\boldsymbol{r},t)$, and $r = \sqrt{x^2+y^2}$,

$$M(\boldsymbol{r}) = \begin{cases} 1, & r \le r_\mathrm{b}, \\ \exp[-\beta(\mathrm{r}-\mathrm{r_b})], & r > r_\mathrm{b}, \end{cases} \tag{7}$$

where $\beta = 1$ a.u., and the boundary between ionized wave function and bounded wave function is $r_\mathrm{b} = 20$ a.u. for the He^+ ion and the H_2^+ molecule, and 30 a.u. for the N_2 molecule. The photoelectron momentum distributions are acquired by Fourier transforming the ionized wave function into momentum space, the photoelectron angular distribution is obtained from the photoelectron momentum distribution.[29]

3. Results and discussion

In the present work, the ultrafast photoionization process of ions and molecules by orthogonally polarized laser pulses with different time delays are presented from numerical solutions of the 2D TDSEs. The PMDs and the PADs of ions and molecules are investigated in orthogonally polarized single color XUV laser fields at wavelengths $\lambda = 15$ nm ($\omega = 3.04$ a.u.). The photon energy $\omega > I_\mathrm{p}$, then the ionization process will occur by absorbing only one photon, which is called the single-photon process, where the Keldysh parameter $\gamma = \sqrt{I_\mathrm{p}/2U_\mathrm{p}} \gg 1$. In addition, the modification of the ionization potential by Stark shift can be ignored.

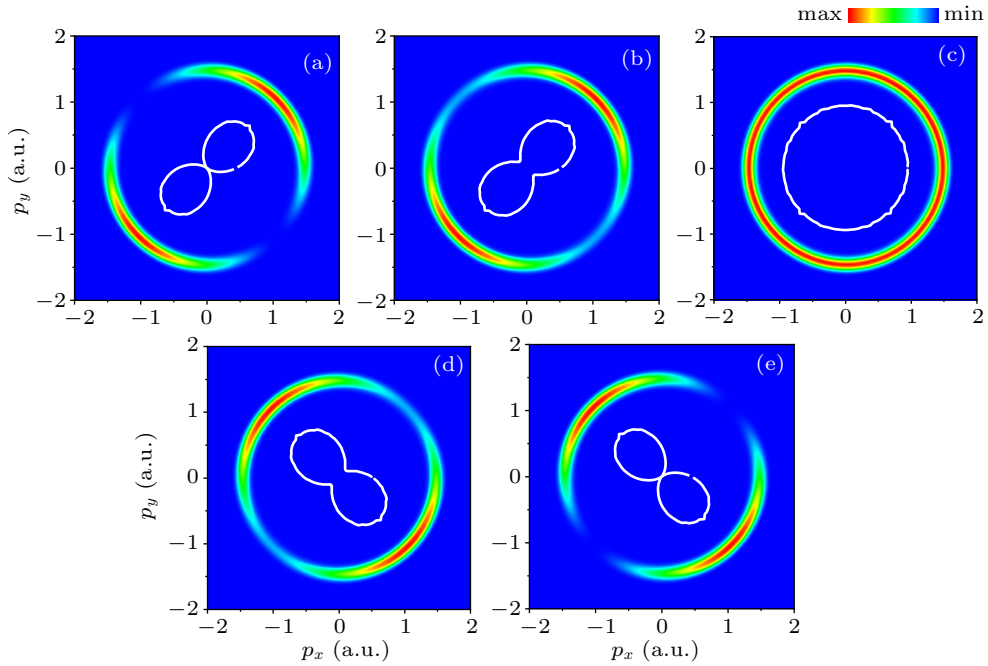


Fig. 2. Two-dimensional PMDs and PADs of He^+ ions by orthogonally polarized laser pulses at $\lambda = 15$ nm ($\omega = 3.04$ a.u.). The intensity of the pulses is $I_0 = 1\times10^{14}$ W/cm^2 ($E_0 = 5.34\times10^{-2}$ a.u.) and duration is 20 optical cycles. The results are shown for time delays: (a) $T_\mathrm{d} = 0$ o.c., (b) $T_\mathrm{d} = 1/8$ o.c., (c) $T_\mathrm{d} = 1/4$ o.c., (d) $T_\mathrm{d} = 3/8$ o.c., and (e) $T_\mathrm{d} = 1/2$ o.c.

We first choose He^+ ion as a benchmark system to describe effects of ionic geometry and the time delay on photoelectron distributions by laser pulses. From Fig. 2 we can see that the PMDs and the PADs are sensitive to the time delay T_d. The PMDs and PADs of He^+ with different time delays (0 o.c., 1/8 o.c., 1/4 o.c., 3/8 o.c., 1/2 o.c.) are shown in Figs. 2(a)–2(e), respectively. According to the energy conservation, with the laser pulse at wavelength

$\lambda = 15$ nm ($\omega = 3.04$ a.u.), the corresponding momentum is $p_{\mathrm{He}^+} = \sqrt{2(\omega - I_\mathrm{p})} = 1.44$ a.u. In Fig. 2(a), at the time delay $T_\mathrm{d} = 0$ o.c., the PMD is mainly localized at momentum $p_x = p_y = \pm 1.02$ a.u. ($p_{\mathrm{He}^+} = 1.44$ a.u.) at angles 45° and 225°. At the time delay $T_\mathrm{d} = 1/8$ o.c., two lobes are located at 45° and 225° with broader distribution and the radius of PAD becomes longer, as shown in Fig. 2(b). At the time delay $T_\mathrm{d} = 1/4$ o.c. in Fig. 2(c), the distribution displays a ring structure with a momentum radius $p_{\mathrm{He}^+} = \sqrt{p_x^2 + p_y^2} = 1.44$ a.u. At the time delay $T_\mathrm{d} = 3/8$ o.c., the PMD is mainly localized at momentum $p_x = p_y = \pm 1.02$ a.u. ($p_{\mathrm{He}^+} = 1.44$ a.u.) at angles 135° and 315°. At the time delay $T_\mathrm{d} = 1/2$ o.c., two lobes are located at 135° and 315° with the narrower distribution and the radius of PAD becomes shorter in Fig. 2(e). It can be seen that the PMDs are sensitive to the time delays.

We adopt the ultrafast photoionization model[25] to describe the interference effects of coherent electron wavepackets in photoelectron momentum and angular distributions, which are dependent on the time delays, the photoionization amplitudes along the x and y directions can then be simply expressed as

$$\mathcal{A}^x_{\mathrm{He}^+}(\theta) \sim \sigma^x f^x(\theta)\Omega(\theta)\psi_{1s}(\boldsymbol{p}), \tag{8}$$

$$\mathcal{A}^y_{\mathrm{He}^+}(\theta) \sim \sigma^y f^y(\theta)\Omega(\theta)\psi_{1s}(\boldsymbol{p}), \tag{9}$$

where $\sigma^x = \sigma^y = 0.00043$ are the ionization probabilities along the x and y directions, the ionization probabilities[31] can be obtained from the initial electronic states of the He^+ ion. A linearly polarized $\lambda = 15$ nm laser pulse is used to ionize these ions. The intensity and duration of the laser pulses are the same as those in Fig. 2. When the field polarized direction is parallel to the x axis, the ionization probabilities σ^x along the x direction is obtained. Similarly, we can obtain the ionization probabilities σ^y along the y direction. The scalar products are $f^x(\theta) = \cos(\theta)$ and $f^y(\theta) = \sin(\theta)$. The wave function ψ_{1s} of the He^+ ion is circular in the (x, y) plane. The interference term of the x and y directions is

$$\begin{aligned}\mathcal{A}^{x,y}_{\mathrm{He}^+}(\theta) &= \mathcal{A}^{x*}_{\mathrm{He}^+}(\theta)\mathcal{A}^{y}_{\mathrm{He}^+}(\theta) + \mathcal{A}^{x}_{\mathrm{He}^+}(\theta)\mathcal{A}^{y*}_{\mathrm{He}^+}(\theta) \\ &= \left\{\sigma^x\sigma^y \sin(2\theta)\cos\left[\left(\frac{p^2}{2} - E_{1s}\right)T_\mathrm{d}\right]\right\}\Omega(\theta).\end{aligned} \tag{10}$$

The corresponding total distributions are

$$\begin{aligned}|\mathcal{A}_{\mathrm{He}^+}(\theta)|^2 &= |\mathcal{A}^x_{\mathrm{He}^+}(\theta)|^2 + |\mathcal{A}^y_{\mathrm{He}^+}(\theta)|^2 + \mathcal{A}^{(x,y)}_{\mathrm{He}^+}(\theta) \\ &= \left\{|\sigma^x\cos(\theta)|^2 + |\sigma^y\sin(\theta)|^2 \right. \\ &\quad + \sigma^x\sigma^y\sin(2\theta)\cos \\ &\quad \left.\times\left[\left(\frac{p^2}{2} - E_{1s}\right)T_\mathrm{d}\right]\right\}\Omega(\theta),\end{aligned} \tag{11}$$

where θ is the angle between the photoelectron momentum $\boldsymbol{p}$ and the x axis. For the He^+ ion, $\Omega(\theta)$ presents circular shape in the (x, y) plane. The term of cosine triangle functions $\cos[(\frac{p^2}{2} - E_{1s})T_\mathrm{d}]$ presents the interference effects of the coherent electron wave packets created by the time delay of two orthogonally polarized laser pulses. In Figs. 3(a)–3(e) we present the theoretical predictions from ultrafast photoionization models in Eq. (11), which are in good agreement with those of TDSE simulations shown in Figs. 2(a)–2(e).

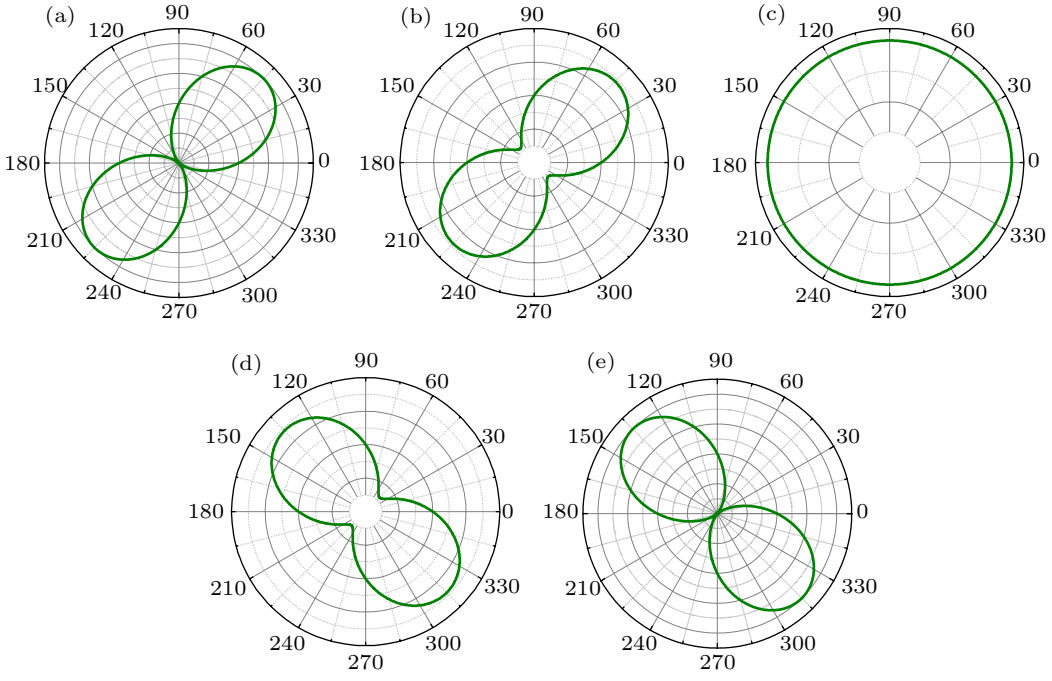


Fig. 3. Predictions of photoelectron angular distributions for He^+ ions obtained from the ultrafast photoionization models in Eq. (11).

The similar phenomenon can be observed in the photoionization process of a linearly molecular system H_2^+. The molecule is aligned along the x axis. The same orthogonally polarized laser pulses with wavelength $\lambda = 15$ nm is used. We present the results from the TDSE simulations in Figs. 4(a1)–4(a3) and the prediction results in Figs. 4(b1)–4(b3). In Fig. 4(a1), at the time delay $T_d = 0$ o.c., two radiation peaks with larger amplitudes are mainly localized at angles 80° and 260°, two radiation peaks with smaller amplitudes are located at angles 8° and 188° as well. At the time delay $T_d = 1/4$ o.c., the PMDs show that two radiation peaks with larger amplitudes are mainly localized at angles 95° and 275°, two radiation peaks with smaller amplitudes are located at angles 8° and 188° in Fig. 4(a2), and a small tilted angle with respect to the laser polarization axis appears. At the time delay $T_d = 3/8$ o.c., two radiation peaks with larger amplitudes are mainly localized at angles 100° and 280°, two radiation peaks with smaller amplitudes are located at angles 172° and 352° in Fig. 4(a3). The wave function of highest occupied molecular orbital (HOMO) for H_2^+ can be simply written as $\psi_{1s\sigma_g} = \psi_{1s}(\boldsymbol{r} - \boldsymbol{R}_e/2) + \psi_{1s}(\boldsymbol{r} + \boldsymbol{R}_e/2)$, which illustrates a linearly combination of 1s atomic orbitals that are located at $\pm R/2$. For an intense laser field, the wave function of the molecules in momentum space is

$$\psi(\boldsymbol{p}, 0^+) = \psi(\boldsymbol{p} + \boldsymbol{E}), \tag{12}$$

where $\psi(\boldsymbol{p}, 0^+)$ is the wave function of the ground electronic state in the momentum $\boldsymbol{p}$ space, and $\boldsymbol{E}$ is the field vector. Transforming the wave function $\psi(\boldsymbol{p}, 0^+)$ to coordinate space, we can obtain

$$\begin{aligned}\psi(\boldsymbol{r}, 0^+) &= (2\pi)^{-3/2} \int \mathrm{e}^{-\mathrm{i}\boldsymbol{p}\cdot\boldsymbol{r}} \psi(\boldsymbol{p}, 0^+) \mathrm{d}\boldsymbol{p} \\ &= \mathrm{e}^{-\mathrm{i}\boldsymbol{E}\cdot\boldsymbol{r}} \psi_0(\boldsymbol{r}).\end{aligned} \tag{13}$$

Then transition amplitude can be given by

$$\begin{aligned}\mathcal{A}(\boldsymbol{p}) &= (2\pi)^{-3/2} \int \mathrm{e}^{-\mathrm{i}\boldsymbol{p}\cdot\boldsymbol{r}} \psi(\boldsymbol{r}, 0^+) \mathrm{d}\boldsymbol{r} \\ &= (2\pi)^{-3/2} \int \mathrm{e}^{-\mathrm{i}\boldsymbol{p}\cdot\boldsymbol{r}} \mathrm{e}^{-\mathrm{i}\boldsymbol{E}\cdot\boldsymbol{r}} \psi_0(\boldsymbol{r}) \mathrm{d}\boldsymbol{r}.\end{aligned} \tag{14}$$

The photoionization amplitudes along the x and y directions can then be simply expressed as

$$\mathcal{A}^x_{H_2^+}(\theta) \sim \sigma^x f^x(\theta) \Omega(\theta) \psi_{1s}(\boldsymbol{p}), \tag{15}$$

$$\mathcal{A}^y_{H_2^+}(\theta) \sim \sigma^y f^y(\theta) \Omega(\theta) \psi_{1s}(\boldsymbol{p}), \tag{16}$$

where $\Omega(\theta)$ is a function of $|\cos[pR_e\cos(\theta)/2]|^2$, and the interference term of the x and y directions is

$$\begin{aligned}\mathcal{A}^{x,y}_{H_2^+}(\theta) &= \mathcal{A}^{x*}_{H_2^+}(\theta)\mathcal{A}^{y}_{H_2^+}(\theta) + \mathcal{A}^{x}_{H_2^+}(\theta)\mathcal{A}^{y*}_{H_2^+}(\theta) \\ &= \sigma^x\sigma^y \sin(2\theta) \cos\left[\left(\frac{\boldsymbol{p}^2}{2} - E_{1s\sigma_g}\right) T_d\right] \\ &\quad \times |\cos[pR_e\cos(\theta)/2]|^2.\end{aligned} \tag{17}$$

The corresponding total distributions can be written as

$$\begin{aligned}|\mathcal{A}_{H_2^+}(\theta)|^2 &= \left\{|\sigma^x\cos(\theta)|^2 + |\sigma^y\sin(\theta)|^2 \right. \\ &\quad \left. + \sigma^x\sigma^y \sin(2\theta)\cos\left[\left(\frac{\boldsymbol{p}^2}{2} - E_{1s\sigma_g}\right) T_d\right]\right\} \\ &\quad \times |\cos[pR_e]\cos(\theta)/2]|^2.\end{aligned} \tag{18}$$

Here, $\sigma^x = 0.0000096$ and $\sigma^y = 0.0000145$ are the ionization probability along the x and y directions. The corresponding photoelectron momentum with the wavelength $\lambda = 15$ nm is $p_{H_2^+} = \sqrt{2(\omega - I_p)} = 1.97$ a.u. The term of cosine triangle functions $\cos[(\boldsymbol{p}^2/2 - E_{1s\sigma_g})T_d]$ present the interference effects of the coherent electron wave packets created by the time delay of two orthogonally polarized laser pulses, and the term of cosine triangle functions $|\cos[pR_e\cos(\theta)/2]|^2$ presents the interference effects of the coherent electron wave packets emanating from the two nuclear centers. The results of photoelectron distributions of H_2^+ is in good agreement with the prediction results of angular nodels obtained from Eq. (18), proving that the ultrafast photoionization model can well interpret photoelectron process of H_2^+.

In order to further understand the effects of the time delays on photoelectron angular distributions of multi-electron molecules, the N_2 molecule is used as a benchmark system in orthogonally polarized laser fields. The N_2 molecule is aligned along the x axis. In Fig. 5(a1), at time delay $T_d = 0$ o.c., PAD is mainly localized at angles 135° and 315°, from Figs. 5(a1)–5(c1) we can see that the PADs for N_2 molecule has four radiation peaks located at angles 38°, 135°, 217°, 315°, and as the time delay increases, the distribution in first and third quadrants in the (x,y) plane becomes weaker, whereas after $T_d = 1/4$ o.c. (as shown in Fig. 5(c1)), the distribution in first and third quadrants becomes broader.

The derivation process of N_2 molecules is same as Eqs. (12)–(14) for H_2^+ molecules. The wave function $\psi_{2p\sigma_g}$ of HOMO for N_2 molecules can be simply written as $\psi_{2p\sigma_g} = \psi_{2p_x}(\boldsymbol{r} - \boldsymbol{R}_{N-N}/2) - \psi_{2p_x}(\boldsymbol{r} + \boldsymbol{R}_{N-N}/2)$, which is a linear combination of $2p_x$ atomic orbitals that are located at $\pm R/2$. The shape of the wave function of the ψ_{2p_x} orbital is proportional to the function of $\cos(\theta)$, and $\Omega(\theta)$ is a function of $|\sin[pR_{N-N}\cos(\theta)/2]|^2$. We take $\sigma^x = 0.0432$ and $\sigma^y = 0.0438$ as the ionization probabilities along the x and y directions. It should be mentioned that the ionization probabilities along the x and y directions are not the same as the total ionization probability. The corresponding photoelectron momentum with the wavelength $\lambda = 15$ nm is $p_{N_2} = \sqrt{2(\omega - I_p)} = 2.22$ a.u. We calculate the ionization probability in different directions in a linearly polarized $\lambda = 15$ nm laser pulse. The intensity and duration of the laser pulses are the same as those in Fig. 2. For the N_2 molecule, the angle-resolved ionization

probability is a function of $\sin(\theta)$, the photoionization amplitudes along the x and y directions can then be simply expressed as

$$\mathcal{A}^{x}_{\mathrm{N}_2}(\theta) \sim \sigma^{x} f^{x}(\theta)\Omega(\theta)\psi_{2p}(\boldsymbol{p}), \tag{19}$$

$$\mathcal{A}^{y}_{\mathrm{N}_2}(\theta) \sim \sigma^{y} f^{y}(\theta)\Omega(\theta)\psi_{2p}(\boldsymbol{p}). \tag{20}$$

The interference term of the x and y directions is

$$\begin{aligned}\mathcal{A}^{x,y}_{\mathrm{N}_2}(\theta) &= \mathcal{A}^{x*}_{\mathrm{N}_2}(\theta)\mathcal{A}^{y}_{\mathrm{N}_2}(\theta) + \mathcal{A}^{x}_{\mathrm{N}_2}(\theta)\mathcal{A}^{y*}_{\mathrm{N}_2}(\theta) \\ &= \sigma^{x}\sigma^{y}\sin(2\theta)\cos\left[\left(\frac{\boldsymbol{p}^2}{2} - E_{2p\sigma_{\mathrm{g}}}\right)T_{\mathrm{d}}\right] \\ &\quad \times |\sin(\theta)\cos(\theta)\sin[pR_{\mathrm{N-N}}\cos(\theta)/2]|^2. \end{aligned} \tag{21}$$

The corresponding total distributions can be written as

$$\begin{aligned}|\mathcal{A}_{\mathrm{N}_2}(\theta)|^2 &= \left\{|\sigma^{x}\cos(\theta)|^2 + |\sigma^{y}\sin(\theta)|^2 \right. \\ &\quad \left. + \sigma^{x}\sigma^{y}\sin(2\theta)\cos\left[\left(\frac{\boldsymbol{p}^2}{2} - E_{2p\sigma_{\mathrm{g}}}\right)T_{\mathrm{d}}\right]\right\} \\ &\quad \times |\sin(\theta)\cos(\theta)\sin[pR_{\mathrm{N-N}}\cos(\theta)/2]|^2. \end{aligned} \tag{22}$$

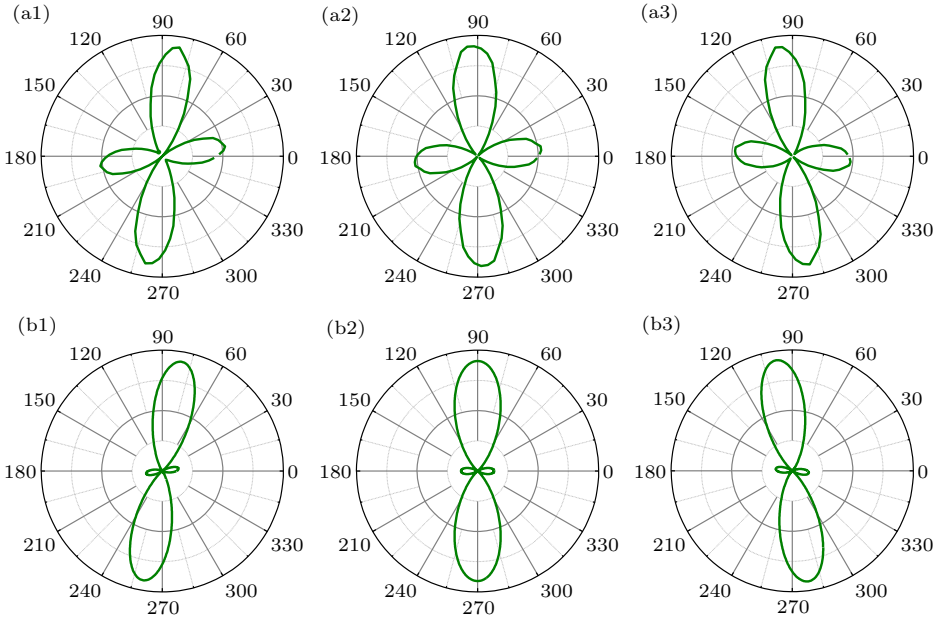


Fig. 4. Two-dimensional PADs of aligned H_2^+ at equilibrium $R_{\mathrm{e}} = 2.0$ a.u. by orthogonally polarized laser pulses at wavelength $\lambda = 15$ nm ($\omega = 3.04$ a.u.). The intensity of the pulses is $I_0 = 1 \times 10^{14}$ W/cm^2 ($E_0 = 5.34 \times 10^{-2}$ a.u.) and duration is 20 optical cycles. The numerical results are shown for time delays: (a1) $T_{\mathrm{d}} = 0$ o.c., (b1) $T_{\mathrm{d}} = 1/4$ o.c., (c1) $T_{\mathrm{d}} = 3/8$ o.c. The prediction results of angular nodels obtained from Eq. (18): (a2) $T_{\mathrm{d}} = 0$ o.c., (b2) $T_{\mathrm{d}} = 1/4$ o.c., (c2) $T_{\mathrm{d}} = 3/8$ o.c.

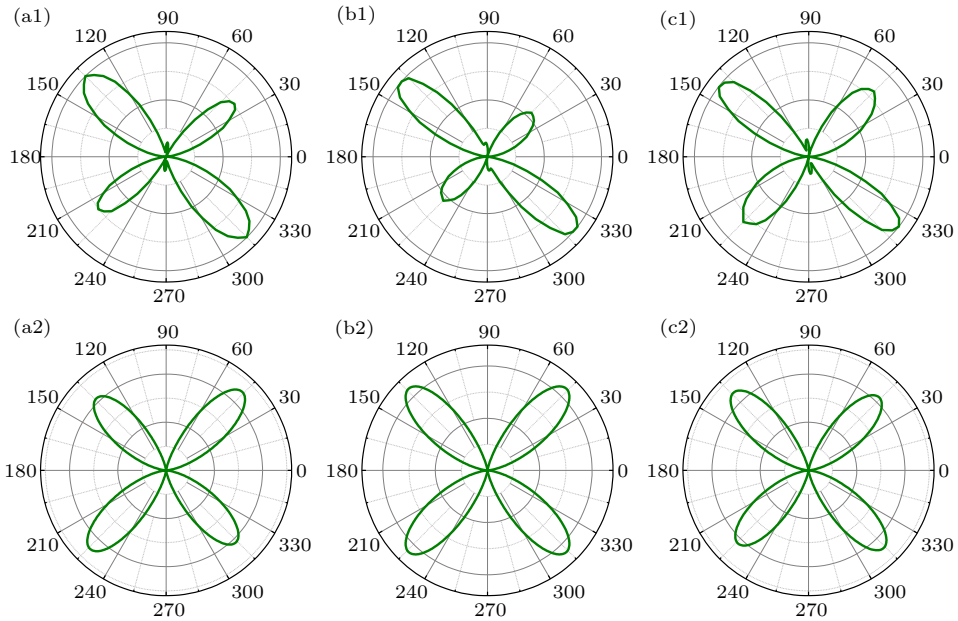


Fig. 5. Two-dimensional PADs of aligned N_2 at equilibrium $R_{\mathrm{N-N}} = 2.08$ a.u. by orthogonally polarized laser pulses at $\lambda = 15$ nm ($\omega = 3.04$ a.u.). The intensity of the laser pulses is $I_0 = 1 \times 10^{14}$ W/cm^2 ($E_0 = 5.34 \times 10^{-2}$ a.u.) and duration is 20 optical cycles. The numerical results are shown for time delays: (a1) $T_{\mathrm{d}} = 0$ o.c., (b1) $T_{\mathrm{d}} = 1/4$ o.c., (c1) $T_{\mathrm{d}} = 3/8$ o.c. The prediction results of angular nodels obtained from Eq. (22): (a2) $T_{\mathrm{d}} = 0$ o.c., (b2) $T_{\mathrm{d}} = 1/4$ o.c., (c2) $T_{\mathrm{d}} = 3/8$ o.c.

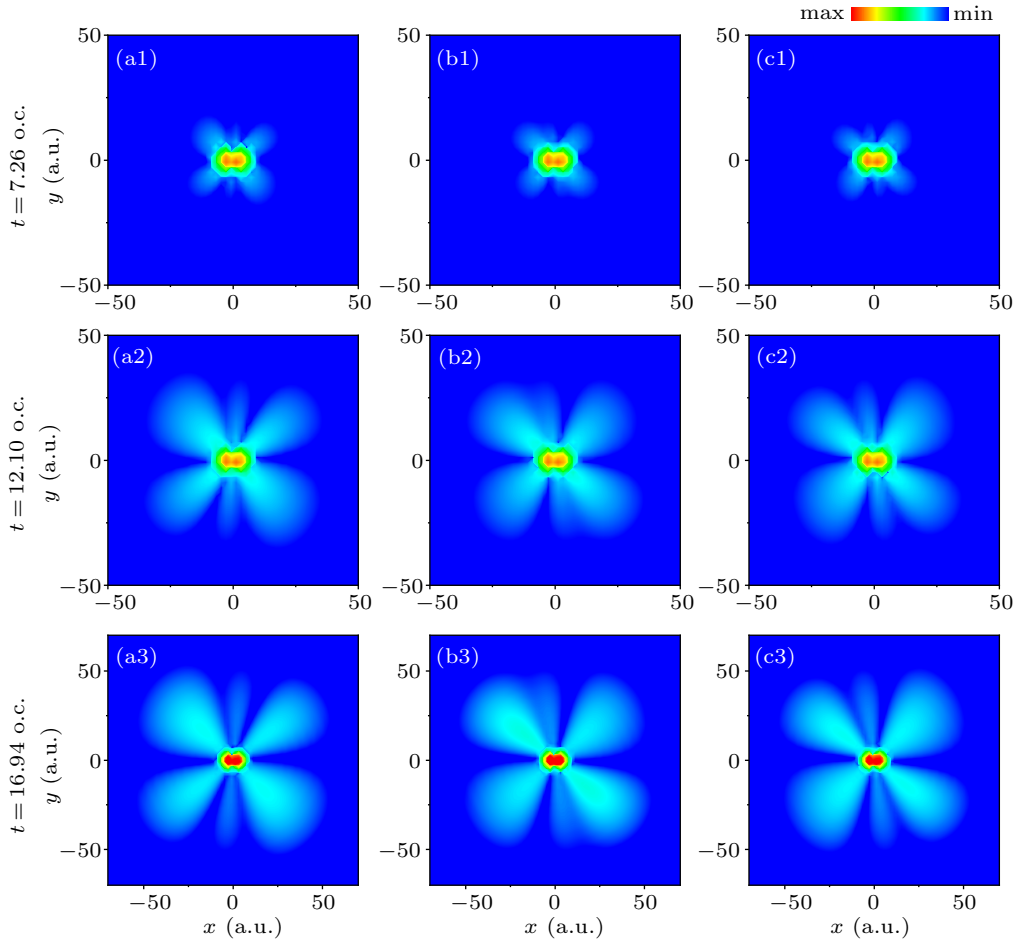


Fig. 6. The electron wavepackets for the N_2 molecules at different times by orthogonally polarized laser pulses at wavelength $\lambda = 15$ nm ($\omega = 3.04$ a.u.) with four time delays: [(a1), (a2), (a3)] $T_d = 0$ o.c., [(b1), (b2), (b3)] $T_d = 1/4$ o.c. and [(c1), (c2), (c3)] $T_d = 3/8$ o.c. The results are shown at four different times: [(a1), (b1), (c1)] $t = 7.26$ o.c., [(a2), (b2), (c2)] $t = 12.10$ o.c. and [(a3), (b3), (c3)] $t = 16.94$ o.c.

The corresponding prediction results obtained from Eq. (22) are presented in Figs. 5(a2)–5(c2). The term of cosine triangle functions $\cos[(\frac{p^2}{2} - E_{2p\sigma_g})T_d]$ presents the interference effects of the coherent electron wave packets created by the time delay of two orthogonally polarized laser pulses, and the term of sine triangle functions $\sin[pR_{N-N}\cos(\theta)/2]$ presents the interference effects of the coherent electron wave packets emanating from the two nuclear centers. The angles of the radiation peaks of the PADs from TDSE simulations and theoretical predictions are identical. However, the intensity of the PADs from the TDSE simulations and theoretical predictions are inconsistent. From Figs. 5(a1)–5(c1), it is found that these PADs exhibit an asymmetry with regard to the molecular axis, i.e. the x axis. At $T_d = 0$ o.c., the distribution is dominant in the second and fourth quadrants in Fig. 5(a1). With T_d increasing, the distribution in the first and third quadrants decreases. At the time delay $T_d = 3/8$ o.c., the distribution in the first and third quadrants increases. However, in view of the prediction result shown in Fig. 5(a2), the amplitudes of two radiation peaks in the second and fourth quadrants are weaker than those in the first and third quadrants. At $T_d = 1/4$ o.c., the prediction result shows symmetric distribution with respect to the molecular axis, as shown in Fig. 5(b2). In Fig. 5(c2), the amplitudes of two radiation peaks in the first and third quadrants are weaker than those in the second and fourth quadrants.

In order to describe the intensity of the PADs for N_2 molecules from the TDSE simulations, the evolution of the electron wavepackets by orthogonally polarized laser pulses with different time delays are shown in Fig. 6. In Figs. 6(a1–6(c1), at $t = 7.26$ o.c., the electrons are not ionized and the electrons distributed around the molecular nucleus. In Figs. 6(a2)–6(c2), at $t = 12.10$ o.c., the electrons have been mainly ionized in four directions, and the electrons distribute in the range from 26° to 58°, from 118° to 167°, from 204° to 238° and from 295° to 338°, which are in agreement with the PADs of N_2 molecules in Fig. 5. In Figs. 6(a3)–6(c3), at $t = 16.94$ o.c., more electrons have been ionized in the (x, y) plane. The electron wavepacket by orthogonally polarized laser pulses with the time delay $T_d = 0$ o.c. at time $t = 16.94$ o.c. is presented in Fig. 6(a3), which shows that there are more electrons distributed in the range from 108° to 167° in the second quadrant and from 292° to 342° in the fourth quadrant rather than the range from 18° to 58° in the first quadrant and from 197° to 241° in the third quadrant. Thus the radius of the PAD for N_2 molecules located at angles 135° and 315° is longer and wider than the radius

located at angles 38° and 217° in Fig. 5(a). The electron wavepacket by orthogonally polarized laser pulses with the time delay $T_d = 1/4$ o.c. at time $t = 16.94$ o.c. is presented in Fig. 6(b3), which shows that there are much more electrons distributed in the range from 118° to 164° in the second quadrant and from 298° to 340° in the fourth quadrant rather than the range from 25° to 61° in the first quadrant and from 206° to 243° in the third quadrant. Thus the radius of the PAD for N_2 molecules located at angles 138° and 318° is much longer than the radius located at 42° and 222° in Fig. 5(b). The electron wavepacket by orthogonally polarized laser pulses with the time delay $T_d = 3/8$ o.c. at time $t = 16.94$ o.c. is presented in Fig. 6(c3), which shows that there are more electrons distributed in the range from 121° to 164° in the second quadrant and from 301° to 342° in the fourth quadrant rather than the range from 22° to 63° in the first quadrant and from 203° to 243° in the third quadrant. Thus the radius of the PAD for N_2 molecules located at 142° and 322° is longer than the radius located at 45° and 224° in Fig. 5(b).

4. Conclusions

The ionic and molecular photoionization in orthogonally polarized laser fields for different time delays is investigated theoretically. Simulations are performed on the He^+ ions, H_2^+ molecules and N_2 molecules by numerically solving corresponding 2D TDSEs. The PMDs and PADs are dependent on the time delays between the orthogonally polarized laser pulses, which comes from the interference between coherent electron wave packets. For the He^+ ions, the interference of the coherent electron wave packets is created by the time delay of two orthogonally polarized laser pulses. For H_2^+ molecules and N_2 molecules, the interference of the coherent electron wave packets is created by the time delay of two orthogonally polarized laser pulses and two-center ionization. The ultrafast photoionization model[25] is adopted to describe these results given above. The PADs of He^+ ions and H_2^+ molecules can be well described by the ultrafast photoionization model, and the angles of the PADs for N_2 molecules from the TDSE simulations are in good agreement with the prediction from the ultrafast photoionization model. The evolution of the electron wavepackets is employed to describe the intensity from TDSE simulations for N_2 molecules.

Acknowledgment

We are thankful to Hongdan Zhang for helping us with the corrections of the article.

References

[1] Zhang J, Qi T, Pan X F, Guo J, Zhu K G and Liu X S 2019 *Chin. Phys. B* **28** 103204
[2] Shao J, Zhang C P, Jia J C, Ma J L and Miao X Y 2019 *Chin. Phys. Lett.* **36** 054203
[3] Taylor J E, Zhang Z, Cao G, Haber L H, Jin R and Plummer E W 2018 *Chin. Phys. Lett.* **35** 097102
[4] Xu T T, Chen J H, Pan X F, Zhang H D, Ben S and Liu X S 2018 *Chin. Phys. B* **27** 093201
[5] Brabec T and Krausz F 2000 *Rev. Mod. Phys.* **72** 545
[6] Agostini P and DiMauro L F 2004 *Rep. Prog. Phys.* **67** 813
[7] Krausz F and Ivanov M 2009 *Rev. Mod. Phys.* **81** 163
[8] von den Hoff P, Znakovskaya I, Kling M F and de Vivie-Riedle R 2009 *Chem. Phys.* **366** 139
[9] Corkum P B and Krausz F 2007 *Nat. Phys.* **3** 381
[10] Shao H C and Starace A F 2010 *Phys. Rev. Lett.* **105** 263201
[11] Hockett P, Bisgaard C Z, Clarkin O J and Stolow A 2011 *Nat. Phys.* **7** 612
[12] Niikura H, Villeneuve D M and Corkum P B 2005 *Phys. Rev. Lett.* **94** 083003
[13] Shao H C and Starace A F 2010 *Phys. Rev. Lett.* **105** 263201
[14] Bandrauk A D, Chelkowski S and Nguyen H S 2004 *Int. J. Quantum Chem.* **100** 834
[15] Chelkowski S, Yudin G L and Bandrauk A D 2006 *J. Phys. B* **39** S409
[16] Djiokap J N, Meremianin A, Manakov N, Madsen L and Hu S and Starace A 2018 *Phys. Rev. A* **98** 063407
[17] Djiokap J N, Meremianin A, Manakov N, Hu S, Madsen L and Starace A 2016 *Phys. Rev. A* **94** 013408
[18] Yuan K J, Chelkowski S and Bandrauk A D 2016 *Phys. Rev. A* **93** 053425
[19] Djiokap J N, Hu S, Madsen L B, Manakov N, Meremianin A and Starace A F 2015 *Phys. Rev. Lett.* **115** 113004
[20] Yuan K J, Lu H and Bandrauk A D 2017 *Struct. Chem.* **28** 1297
[21] Yuan K J, Chelkowski S and Bandrauk A D 2015 *Chem. Phys. Lett.* **638** 173
[22] Richter M, Kunitski M, Schöffler M, Jahnke T, Schmidt L P H, Li M, Liu Y and Dörner R 2015 *Phys. Rev. Lett.* **114** 143001
[23] Li M, Jiang W C, Xie H, Luo S, Zhou Y and Lu P 2018 *Phys. Rev. A* **97** 023415
[24] Yuan K J, Chelkowski S and Bandrauk A D 2017 *Chem. Phys. Lett.* **683** 639
[25] Zuo T, Bandrauk A D and Corkum P B 1996 *Chem. Phys. Lett.* **259** 313
[26] Peters M, Nguyen-Dang T, Charron E, Keller A and Atabek O 2012 *Phys. Rev. A* **85** 053417
[27] Bandrauk A D and Shen H 1993 *J. Chem. Phys.* **99** 1185
[28] Bandrauk A D and Lu H 2013 *J. Theor. Comput. Chem.* **12** 1340001
[29] Zhang H D, Ben S, Xu T T, Song K L, Tian Y R, Xu Q Y, Zhang S Q, Guo J and Liu X S 2018 *Phys. Rev. A* **98** 013422
[30] Zhu X, Liu X, Li Y, Qin M, Zhang Q, Lan P and Lu P 2015 *Phys. Rev. A* **91** 043418
[31] Odenweller M, Takemoto N, Vredenborg A, Cole K, Pahl K, Titze J, Schmidt L P H, Jahnke T, Dörner R and Becker A 2011 *Phys. Rev. Lett.* **107** 143004